

Variational Autoencoders for Anomalous Jet Tagging

Taoli Cheng

*Mila – Quebec Artificial Intelligence Institute,
6666 St-Urbain, #200, Montreal, QC, H2S 3H1, Canada and
Department of Informatics, Université de Montréal*

Jean-François Arguin, Julien Leissner-Martin, Jacinthe Pilette

*Département de physique, Université de Montréal,
Complexe des Sciences, Case postale 6128,
succursale Centre-ville, Montréal (Québec) H3C 3J7, Canada*

Tobias Golling

*Department of Particle Physics, University of Geneva, 24,
quai Ernest-Ansermet, CH-1211 Genève 4, Switzerland*

Abstract

We present a detailed study on Variational Autoencoders (VAEs) for anomalous jet tagging. By taking in low-level jet constituents' information, and only training with background jets in an unsupervised manner, the VAE is able to encode important information for reconstructing jets, while learning an expressive posterior distribution in the latent space. When using VAE as an anomaly detector, we present two approaches to detect anomalies: directly comparing in the input space or, instead, working in the latent space. Different anomaly metrics were examined. Results of the tagging performance for different jet types and over a large kinematic range are shown. In order to facilitate general search approaches such as bump-hunt, mass-decorrelated VAEs based on distance correlation regularization are also examined. Confronted with the problem of mis-assigning lower likelihood to out-of-distributions samples, we explore one potential solution – Outlier Exposure (OE). OE, in the context of jet tagging, is employed to facilitate two goals: increasing sensitivity of outlier detection and decorrelating jet mass. We observe excellent results from both aspects. Code implementation can be found in [Github](#).

I. INTRODUCTION

Supervised classifiers that are based on deep neural networks have been used for boosted jet tagging and have become a mature research topic in the past few years. It's also worth exploring other methods beyond the specific supervised taggers. The goal is to be able to tag new physics signals in a model-independent manner in the hope of simple execution and high performance. For model-motivated new physics searches, only null results have been obtained so far at the LHC. At the same time, model-independent and data-driven methods, especially assisted by modern machine learning approaches, are becoming potential alternative search strategies. In particular, unsupervised learning methods has become more popular in the field of new physics search at the LHC. Unsupervised learning methods including clustering, density estimation, etc. have been used in the general scope of detecting novel or anomalous events. Anomaly detection methods for LHC physics [1–5] including density estimation, weakly-supervised classification, etc. have been studied recently.

Transitioning from traditional density-based or distance-based anomaly detection, deep generative models succeed in modeling complex high-dimensional density distributions, and are thus used to process high-dimensional data. We can utilize unsupervised training of deep generative models for anomalous jet tagging, while intaking all low-level features, and being as model-independent as possible. Autoencoders (AEs) and Variational Autoencoders (VAEs) have been explored for new physics searches recently. Autoencoder-based anomaly detection has been used in anomalous jet tagging [6–9]. Variational Autoencoders are also explored for event selection at the LHC [10]. Some of them are working on high-level features, while others are working on low-level jet constituents instead. These models are trained with only background data, and at test time are used to detect signals as anomalies. For anomalous jet tagging, autoencoders trained with only QCD jets are used to detect non-QCD jets such as boosted top jets. Autoencoders employ a bottleneck architecture to effectively reduce the data dimensionality, and by using the bottleneck, extract relevant information for reconstructing input features. Using either images or four vector-based input features, autoencoders have been shown to be potential in detecting heavy resonances [6, 7]. The basic idea of using autoencoder as anomaly detector is assuming that the trained AEs will be able to reconstruct samples similar to training samples (*in-distribution*, InD), while giving large reconstruction errors when applied to unseen datasets (*out-of-distribution*, OoD). Thus the

reconstruction error has been used as the anomaly score in most of the literature to date. At the same time, adversarial training to decorrelate jet mass from the reconstruction error has been explored to assist bump-hunt based new physics searches [6]. In Fig. 1, we depict the schematics for AE-based anomalous jet tagger. Jet reconstruction is encouraged by minimizing the reconstruction error between input and output samples. The latent space of deterministic AEs is not taken as optimization targets, thus is not ready for direct use and has random behaviour (see Fig. 1). A simple idea of regularizing the latent space will lead us to Variational Autoencoders [11]. Migrating from deterministic Autoencoders to Variational Autoencoders for anomalous jet tagging, there are a few motives: regularized and expressive latent representations; combined with generative models and maximum likelihood estimation. As indicated in Fig. 2, VAE has a regularized latent distribution imposed by minimizing divergence in latent space, in addition to minimizing reconstruction error in input space is the case for deterministic AEs.

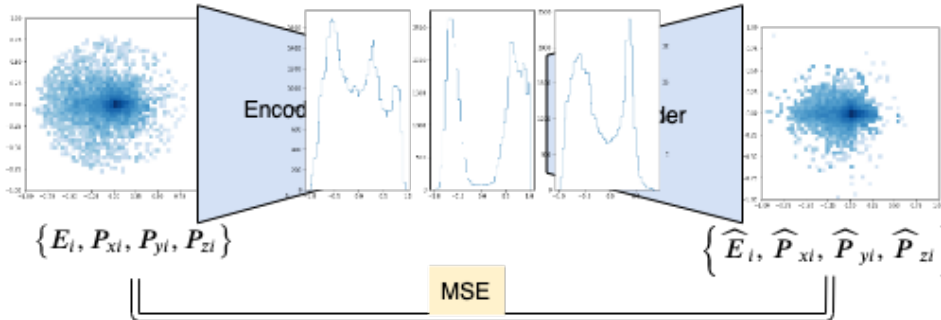


FIG. 1: Schematics of Autoencoder-based anomalous jet tagger. Jet reconstruction is encouraged by minimizing the reconstruction error between outputs $\{\hat{E}_i, \hat{P}_{xi}, \hat{P}_{yi}, \hat{P}_{zi}\}$ and inputs $\{E_i, P_{xi}, P_{yi}, P_{zi}\}$.

Despite the fact that generative models provide us a simple approach for dealing with high-dimensional anomaly detection, they are not guaranteed to succeed for all use-cases. For instance, QCD jets might be assigned larger reconstruction error or lower likelihood than a W jet with two-prong structure, as will be shown later. These problems are also encountered in the general domain of anomaly detection in the machine learning community. For instance, in anomaly detection of natural images, it was found that higher probability is sometimes assigned to outliers than in-distribution samples [12, 13]. The pixel-space similarity is still not mature enough to render robust representation learning. And sometimes background

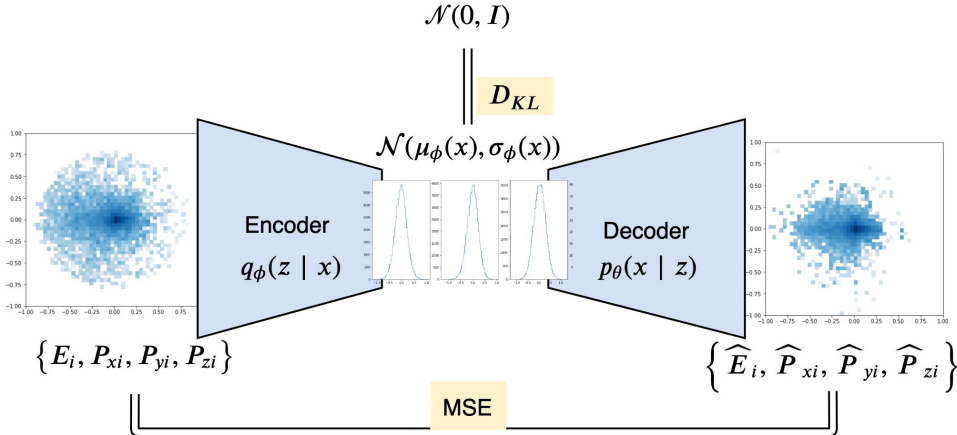


FIG. 2: Schematics of Variational Autoencoder-based anomalous jet tagger. Both the reconstruction error between outputs and inputs and the divergence of latent distributions are required to be optimized.

confounding also brings spurious correlation that handicaps the OoD detection.

In this work, we base our anomalous jet tagging on the framework of VAEs, with possibilities of utilizing anomaly metrics in both input space and latent space. Based on the previously mentioned motivations and existing problems, we examine every building block in the process of using VAEs for anomalous jet tagging. We first construct a basic VAE model for low-level constituents-based jet taggers. In order to ensure that we have a fully-performing generative model, we examine its reconstruction performance, generation performance, and also the latent space. To have a fair assessment of the anomaly detection performance, we tailor a series of test jet sets spanning in the range of different jet masses and jet types. Other than reconstruction loss used in corresponding deterministic AEs applications, we examine a few alternatives for anomaly metrics. In large-radius jet-based new physics searches such as bump-hunt, having a mass-decorrelated tagger will be beneficial. We thus implement a mass-decorrelated VAE tagger with the help of a regularization approach [14], which is faster and easier to train than an auxiliary adversarial network.

Outlier Exposure (OE) [13] is proposed to solve the probability mis-assignment problem (i.e. outliers are assigned higher probability), as mentioned before. By injecting a few samples of outliers, it helps the autoencoder get better separation for InD samples and OoD samples. It is also reported that it generalizes to other OoD distributions. Furthermore, the auxiliary task of OE also provides us a very good handle to shape the latent manifold

tailored to our tasks. Actually, we employ outlier exposure not only as an inducer for detecting sensitivity of unseen outlier samples, but also as a tool to shape the information encoded. Using outlier samples as a handle, we achieve decorrelation effects by using equivalent “planning” [15, 16] (or, reweighting samples to obtain identical distributions) in jet mass. We achieve very good mass decorrelation by matching mass distributions between exposed outlier dataset and in-distribution dataset, while at the same time gaining promising sensitivity for most jet types.

The paper is organised as follows: in Section II we present the basic settings of the problem and examine the properties of trained VAE models; in Section III the performance of detecting non-QCD jets is carefully investigated; mass-decorrelated taggers are introduced and studied in Section IV; an outlier exposure solution to sensitivity and mass-decorrelation is presented in Section V; finally we summarize this work in Section VI.

II. VARIATIONAL AUTOENCODER FOR ANOMALOUS JET TAGGING

We provide here some mathematical foundation of VAEs [11]. As briefly mentioned in the introduction, VAEs can be viewed as the regularized version of deterministic AEs by imposing latent structure with a Kullback–Leibler divergence (KL divergence, D_{KL}) from prior distribution to posterior distribution for latent variables. Practically speaking, a VAE, similar to an AE, consists of an encoder and a decoder, which are both parametrized with neural networks. By parametrizing the variational inference and generative model with deep neural networks, mapping input data X ($X \in \mathcal{X}$) into the latent space with $Q(z|X)$ and mapping the latent representation z back into the input space with $P(X|z)$; the training objective of VAEs includes an extra term of minimizing divergence between prior $P(z)$ and posterior $Q(z|X)$ distributions of latent variables z . Despite the fact that VAE is a deep generative model, it trains fast by simple back-propagation with a re-parametrization trick. The re-parametrization instead reparametrizes the sampling using an extra input layer.

The actual objective of the VAE is to approximately maximize the log-likelihood $\log P(X)$, within a Bayesian inference framework. The log-likelihood of the input data distribution can be written in terms of:

$$\log P(X) - D_{\text{KL}}[Q(z|X)||P(z|X)] = \mathbb{E}_{z \sim Q}[\log P(X|z)] - D_{\text{KL}}[Q(z|X)||P(z)], \quad (1)$$

in which $\mathbb{E}_{z \sim Q}[\log P(X|z)]$ is empirically the reconstruction error of an autoencoder. The left-hand side of Eq. 1 is the marginal log-likelihood we want to maximize (the other divergence term can be effectively minimized in the case of a powerful decoder Q). The right-hand side of Eq. 1 is called *Evidence Lower BOund* (ELBO), since it gives a lower bound of the log-likelihood. ELBO is just the VAE objective and practically the sum of reconstruction error of the autoencoder and the distance between posterior and prior distributions in the latent space.

So empirically the training objective of the VAE can be written as:

$$\mathcal{L}_{\text{VAE}} = \mathcal{L}_{\text{recon}} + \mathcal{L}_{\text{KL}} \quad (2)$$

From another point of view, VAEs can be seen as a regularized version of deterministic Autoencoders. By imposing explicit constraints in the form of the latent prior distribution, we have a handle of how the latent variables behave. Then the training of VAEs include matching the posterior to the prior distribution by minimizing the KL-divergence from prior to posterior distributions in latent space.

The encoder and decoder inside a VAE serve as inference network and generative network respectively. The latent space from the encoding process provides the posterior latent representation. In standard VAEs, prior latent distributions are assumed to be standard Gaussians $\mathcal{N}(0, I)$. And posteriors are estimated in the form of $\mathcal{N}(\mu(X), \sigma(X))$ by mapping input data points to means and variances of posterior Gaussians. Then z is sampled from this posterior and then mapped back into \mathcal{X} . On the other hand, sampling from latent distribution will be able to generate new samples. So examining the quality of the generated samples also serves as an important metric for how well the VAE is trained.

A. Neural Network Architecture

a. Datasets We train on QCD jets collected from fatjet trigger criteria of ATLAS Collaboration. ¹ QCD di-jet events are generated with MadGraph [17] for LHC 13 TeV, followed by Pythia8 [18] and Delphes [19] for parton shower and fast detector simulation, respectively. No pile-up was simulated. All jets are clustered using the anti-kt algorithm

¹ <https://twiki.cern.ch/twiki/bin/view/AtlasPublic/JetTriggerPublicResults>

[20] with cone size $R = 1.0$, triggered with $p_T > 450$ GeV. Particle flow objects are used for jet clustering, with no jet trimming applied.

b. Input features and Preprocessing We take the first 20 hardest (p_T ordered) jet constituents as inputs in the format of four vectors $\{x_i = (E_i, P_{xi}, P_{yi}, P_{zi}); i = 1, \dots, 20\}$. The number of input jet constituents 20 is chosen to optimize the signal significance of boosted Top jets. Jets are preprocessed with minimum transformations to avoid designing effects. Jet constituents are boosted back to the jet rest frame and centered at $(0, 0)$ in the (η, ϕ) plane. Jets are also rotated so that the jet principal axis $(\sum_i \frac{\eta_i E_i}{R_i}, \sum_i \frac{\phi_i E_i}{R_i})$ (with $R_i = \sqrt{\eta_i^2 + \phi_i^2}$) is vertically aligned on the (η, ϕ) plane, with the rotation angle α indicated in Eq. 3:

$$\tan \alpha = \frac{\sum_i \frac{\phi_i E_i}{R_i}}{\sum_i \frac{\eta_i E_i}{R_i}} \quad (3)$$

c. VAE Architecture We explored two simple architectures: Fully Connected Networks (FCN) and Long Short-Term Memory (LSTM) Networks. Since no significant difference in performance was observed, we only present the results for FCN-VAEs in this paper.

For FCN-VAEs, simple dense layers are employed. ReLU activations are used through latent layers, and linear activation is used in the output layer. Encoder and decoder have symmetric architectures, as the encoder is composed of 256, 128, 64 neurons for each hidden layer. The latent dimension has been optimized to maximise boosted Top signal significance. The Gaussian parameters μ and σ are parametrized by dense layers. Then latent vector z sampled from the posterior distribution $\mathcal{N}(\mu, \sigma^2)$ is passed to the decoder to reconstruct the output jet. A brief summary of the VAE architecture is depicted in Fig. 3. The reconstruction error is simply chosen as Mean Squared Error (MSE) between input features $\{x_i; i = 1 \dots n\}$ and output features $\{\hat{x}_i; i = 1 \dots n\}$, as shown in Eq. 4.

$$\mathcal{L}_{\text{VAE}} = \mathcal{L}_{\text{recon}} + \mathcal{L}_{\text{KL}} = \frac{1}{n} \sum_{i=1 \dots n} \|\hat{x}_i - x_i\|^2 + D_{\text{KL}}(q(z|x) \| p(x)) \quad (4)$$

B. Regularization in the Latent Space

As introduced above, KL divergence in the VAE objective can also be viewed as a regularization term. The VAEs with variable regularization weight other than 1 are also formulated as β -VAE [21] models. To clarify this process, the empirical objective of a VAE is written

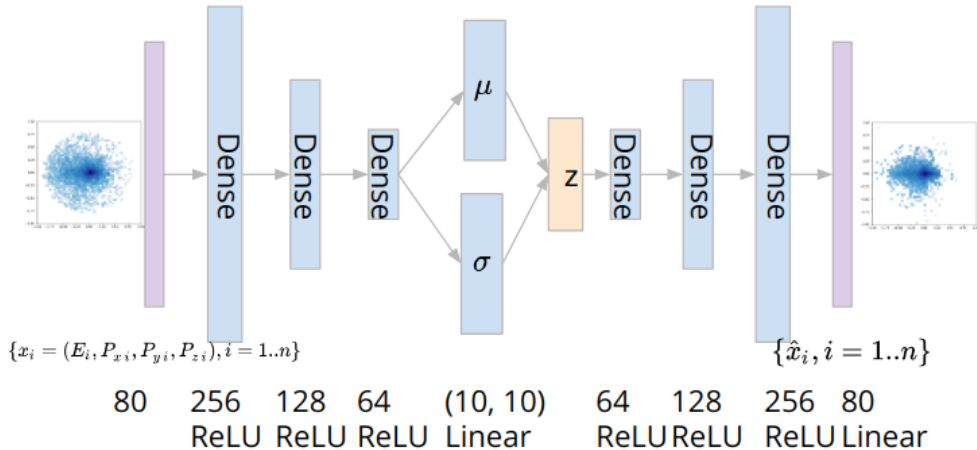


FIG. 3: Architecture of FCN-VAE.

as:

$$\mathcal{L}_{\beta\text{-VAE}} = -\mathbb{E}_{z \sim Q}[\log P(X|z)] + \beta D_{\text{KL}}[Q(z|X) \| P(z)] = \mathcal{L}_{\text{recon}} + \beta \mathcal{L}_{\text{KL}}, \quad (5)$$

where β is the parameter to denote the relative strength of the latent regularization. Setting β affects the competition between fitting the latent distribution and the input space reconstruction. As will be shown later, with $\beta = 0$ the VAE reduces to deterministic autoencoder, for which only the reconstruction is optimized during training, resulting in very good jet reconstruction, however, losing inference capability in the latent space. Increasing β leads to compensation between the jet reconstruction and the latent distribution matching. We have tested different values $\beta = 0.1, 0.5, 1.0, 5.0$, and found that $\beta = 0.1$ gives better balance between reconstruction and latent coding. Throughout this paper, we focus on reporting results for $\beta = 0.1$.

a. Training Setup Throughout this study, we train on 600,000 QCD jets, of which 20% serves as the validation set. We employ Adam [22] for optimization, with the default values of parameters. VAEs are trained for 50 epochs with a batch size of 100.

C. Examining trained VAEs

We examine a few properties of the trained VAE models: jet reconstruction, jet generation, and latent representations.

a. Jet Reconstruction To examine how well QCD jets can be reconstructed by autoencoders, we show a few distributions of reconstructed high-level jet features in Fig. 4. Jet p_T and mass are both well reconstructed.

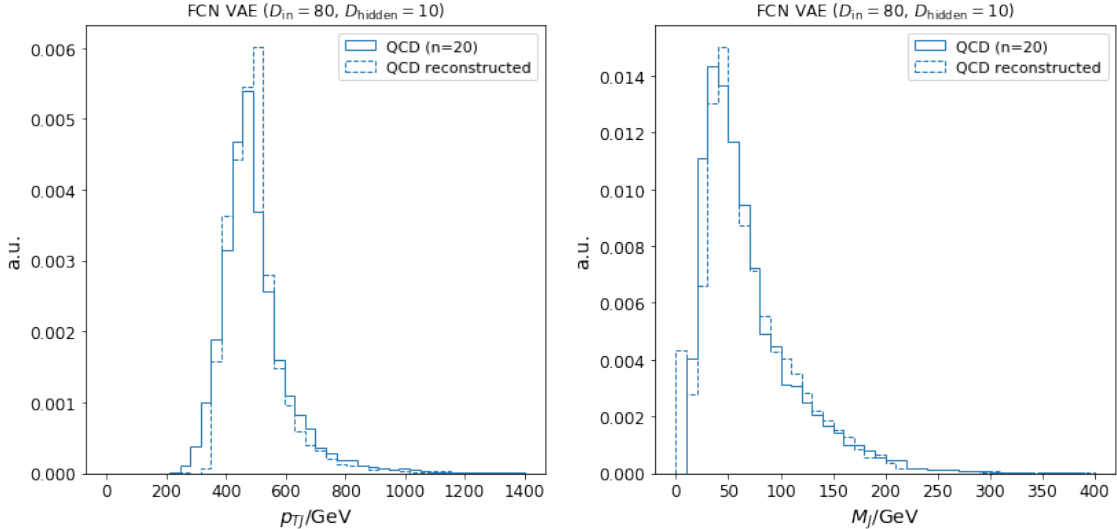


FIG. 4: Reconstructed (dashed lines) Jet p_T and M_J , compared with input jets distributions (solid lines) plotted for first 20 jet constituents with p_T -ordering.

b. Jet Generation To assess the quality of the generative model, we sample from the prior distribution $\mathcal{N}(0, I)$ in the latent space and generate output jets by passing the sampling through the decoder. We show that decoded outputs resemble input distributions.

In Fig. 5, we show aggregated distributions of generated features in the input space (after standardization of input features to be $\sim \mathcal{N}(0, I)$) and jet images on the (η, ϕ) plane. The generated features follow standard Gaussian distributions as we standardized the input features. Generated jet p_T and M_J distributions are shown in Fig. 6. Both generated p_T and M_J distributions match well with the original QCD dataset. However, jet mass is not as perfectly matched, suggesting that the architecture could be further optimized.

c. β -VAE Latent Representation As discussed previously, β controls the balance between reconstruction and latent coding. When β increases, the reconstruction performance drops since there is extra effort to fit the latent distribution. When β is small, it approaches the behaviour of deterministic autoencoders, in the sense that the regularization strength is weak. In Fig. 7, results for $\beta = 0.1$ are shown. We plot the correlation between reconstruction error and jet mass, the correlation between latent KL divergence and jet mass, the

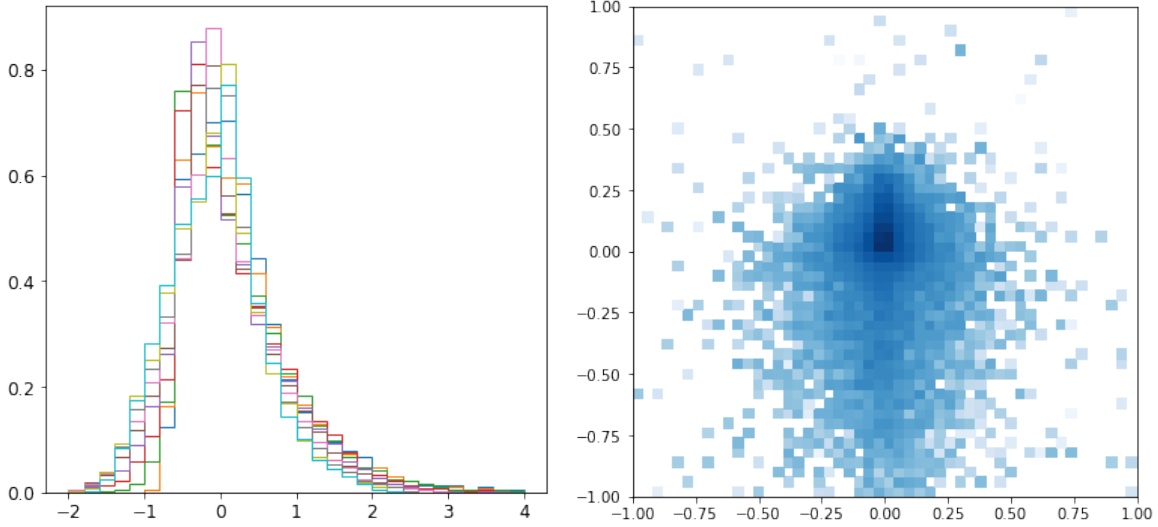


FIG. 5: **Left:** VAE generated input space (scaled) feature distributions. **Right:** VAE generated jet images on the (η, ϕ) plane.

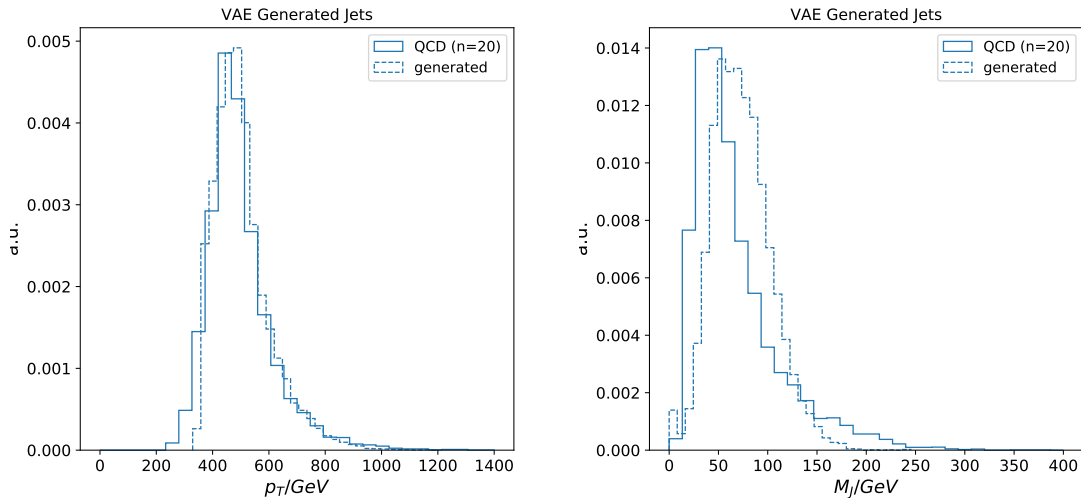


FIG. 6: High level feature distributions of VAE generated jets. **Left:** p_T ; **Right:** M_J .

correlation between reconstruction error and latent KL divergence, and the 2d-tSNE [23] (perplexity = 50) visualisation for mean values of latent representations for in-distribution QCD jets (Blue), out-of-distribution W jets (Green), and Top jets (Orange). First of all, we observe that the reconstruction error has an upper-bounded correlation with jet masses. And the latent KL divergence is also (even more strongly) correlated with jet mass. This suggests that the regularized latent space has encoded relevant information but has different

geometry w.r.t. the input space. Little clustering effect is present in 2d-tSNE visualisation. As β increases (see App. A), a stronger clustering effect is observed at the cost that reconstruction is less maintained.

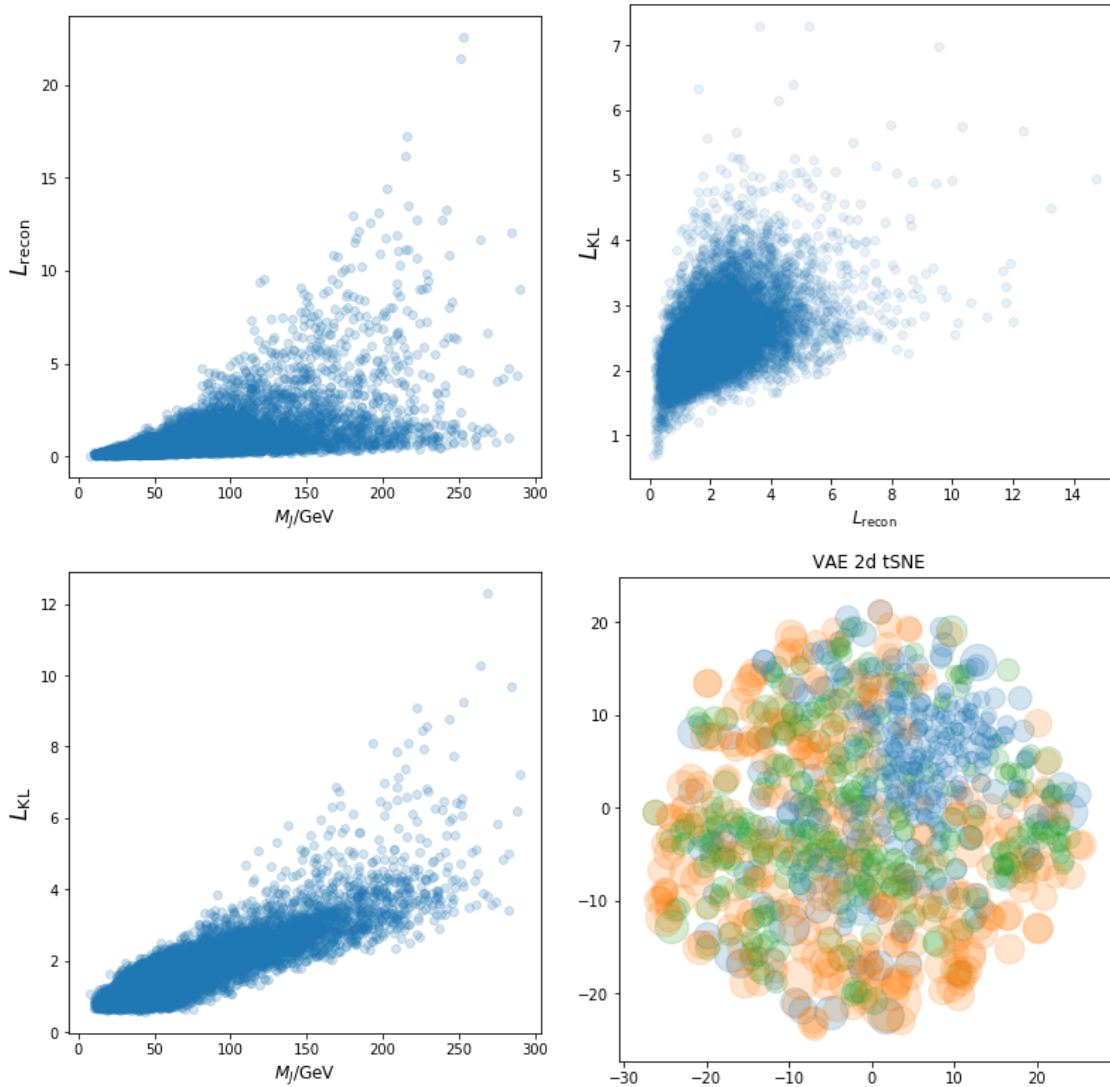


FIG. 7: **Upper-Left:** Reconstruction error vs jet mass; **Upper-Right:** KL divergence vs reconstruction error; **Lower-Left:** KL divergence vs jet mass; **Lower-Right:** Latent 2d-tSNE for different jet types (QCD jets (Blue), W jets (Green) and Top jets (Orange)). All plots are for $\beta = 0.1$.

III. PERFORMANCE IN ANOMALOUS JET TAGGING

In this section, we present the performance of VAE-based anomaly taggers, tested on different jet types, and the responses on jet kinematics. ROC curves and AUCs are used for measuring the performance universally.

a. Test Datasets A series of test sets are generated to examine the detecting performance of VAE-based anti-QCD jet tagging. Boosted W jets, top jets, and Higgs jets are generated as representatives of two-prong, three-prong, and four-prong jets. To test jet mass effects, we composed W jet datasets with rescaled W jet masses (SM W jets with only the mass changed for event generation) for comparison. The same mass-rescaling strategy is also applied to top jets. We employ Two Higgs Doublet Models (THDMs) [24] for generating boosted Higgs jets. Heavy Higgs bosons are generated in pairs ($pp \rightarrow HH$), with decaying into light Higgs pairs. The light Higgs bosons are then restricted to the $h \rightarrow b\bar{b}$ decay mode. Different light Higgs masses are experimented to show different degrees of “four-prongness”. With a very light m_h , boosted heavy Higgs jets will resemble two-pronged jets more. All jets are clustered using anti-kt algorithm with a cone size of $R = 1.0$. When testing on these datasets, jet p_{T} s are restricted to [550, 650] GeV for a fair comparison. The test set size for each jet category is set to be 20,000.

We list here the basic information of test sets:

- Two-prong: boosted W jets are produced by the decay of a heavy resonance W' with $m_{W'} = 1.2$ TeV, $pp \rightarrow W' \rightarrow W(jj), Z(\nu\nu)$, with W decaying to light quark jets and Z decaying to neutrinos. Masses experimented include $m_W = 59, 80, 120, 174$ GeV.
- Three-prong: top jets are generated with the decay of a heavy resonance Z' of $m_{Z'} = 1.3$ TeV, $pp \rightarrow Z' \rightarrow t\bar{t}$. “Top” masses are set to be $m_t = 80, 174$ GeV. (for $m_t = 80$ GeV, the decay product W mass is set to be 20 GeV).
- Four-prong: boosted heavy Higgs pair production is borrowed to generate four-prong samples, $pp \rightarrow HH$, with $H \rightarrow h(bb)h(bb)$ and $m_H = 174$ GeV, $m_h = 20, 80$ GeV. In events generation, we employ h3 in THDM as the heavy Higgs, and h1 as the light Higgs.

A. Anomaly Metric

After successfully training of the VAEs, utilizing the trained models as anomalous jet taggers also requires a good anomaly metric well-defined.

As mentioned above, reconstruction-based anomaly metric has disadvantages when confronted with specific OoD data samples. Even though being the most widely used anomaly metric in the literature, the simple MSE based anomaly metric has a few disadvantages: there is some correlation with jet constituent numbers, although in fixed input length this effect would be eliminated somehow; and strong mass correlation is generally present. Such effects might be better controlled using an anomaly metric based on the low-dimensional latent representations since the data geometry is expected to be much simpler in that space. We thus explored how the KL divergence from prior to posterior distribution in the latent space works as an anomaly metric. Other than that, the negative log-likelihood (NLL) is also directly considered as an anomaly score. Independently from the VAE setting, an optimal transport based metric [25] measuring similarities between input jets and reconstructed jets is also tested as an anomaly score. Besides these machine learning based metrics, we found that a simple Gaussian model for low-level input features already works well. With proper preprocessing, it effectively builds a Gaussian model for input features. Here is a summary of the options investigated as anomaly metrics:

- Negative log-likelihood: $L_{\text{VAE}} = L_{\text{recon}} + L_{\text{KL}}$.
- MSE reconstruction error in input space: $\mathcal{L}_{\text{recon}} = \frac{1}{n} \sum_i \|\hat{x}_i - x_i\|^2$.
- KL divergence in latent space: $L_{\text{KL}} = D_{\text{KL}}(q_\phi(z|x)||q(z))$.
- Energy Mover’s Distance (EMD): EMD is defined as a metric in the collider space using optimal transport to find the minimum energy moving strategy between two LHC events. The EMD between event \mathcal{E} and \mathcal{E}' is defined as:

$$\text{EMD}(\mathcal{E}, \mathcal{E}') = \min_{f_{ij}} \sum_{ij} f_{ij} \frac{\theta_{ij}}{R} + \left| \sum_i E_i - \sum_j E'_j \right|, \quad (6)$$

$$f_{ij} \geq 0, \sum_j f_{ij} \leq E_i, \sum_i f_{ij} \leq E'_j, \sum_{ij} f_{ij} = E_{\min}.$$

where θ_{ij} is the angular distance between particles indexed with i and j in \mathcal{E} and \mathcal{E}' , and f_{ij} denotes the energy being moved between events. $E_{\min} = \min\{\sum_i E_i, \sum_j E'_j\}$. R is

a weight parameter and is set to be 1.0 in our practice. We calculate EMDs between input jets and output jets as the anomaly score. We thus expect out-of-distribution jets will give larger EMDs in the sense that they will not be easily reconstructed. We have already normalized jet p_{TS} to eliminate the contribution from pure energy difference in the second term of Eq. 6.

- **MSS**: simple mean squared sum after standardizing input features to be $\sim \mathcal{N}(0, I)$: $\frac{1}{n} \sum_i \|x_i\|^2$. This can be seen as the simple χ^2 of standardized input features.

B. Results

We first present the ROC curves for NLL based anomaly score. This is aiming at seeing the general responses on different jet types. In Fig. 8, ROC curves under NLL are presented for different test jet types. From the plot, it’s obvious that the VAE performance in the value of the AUC is correlated with jet mass as expected. For mass-rescaled W jets and Top jets, they all show the same trend. As for the jet complexity, we take the jet mass of 174 GeV as a benchmark (**red** lines). We observe that Top jets have the highest discriminative scores, while W and Higgs jets have slightly lower AUCs.² In the rest frame of the heavy Higgs, light Higgs jets with a very small mass are almost produced back to back and are very boosted. Thus h3 with decaying product h1 of a mass of 20 GeV should behave similarly to two-prong jets. From Fig. 8, **h3(h1=20GeV)** has a lower AUC w.r.t. **h3(h1=80GeV)**, as expected. As a conclusion, there is limited yet manifested correlation with jet “complexity”.

Then we focus on examining different anomaly metrics. In Fig. 9, we show results for the other anomaly metrics introduces previously. From the AUC numbers, they all perform similarly. And the mass correlation trend holds for all metrics. Respectively speaking, **MSE** and **EMD** performs most similar. Especially for **KL** and **MSS**, the differences coming from jet types are reduced w.r.t. the other two metrics, while the mass correlation effect is even more obvious. As shown in last section, the **KL** divergence is strongly correlated with the jet mass, which coincides with this observation. In real applications, one will need to choose an anomaly score according to the specific problem at hand.

Since the mass correlation is obvious, low-mass jets generally give low AUCs. This brings

² This might be because we tuned a few parameters according to top.

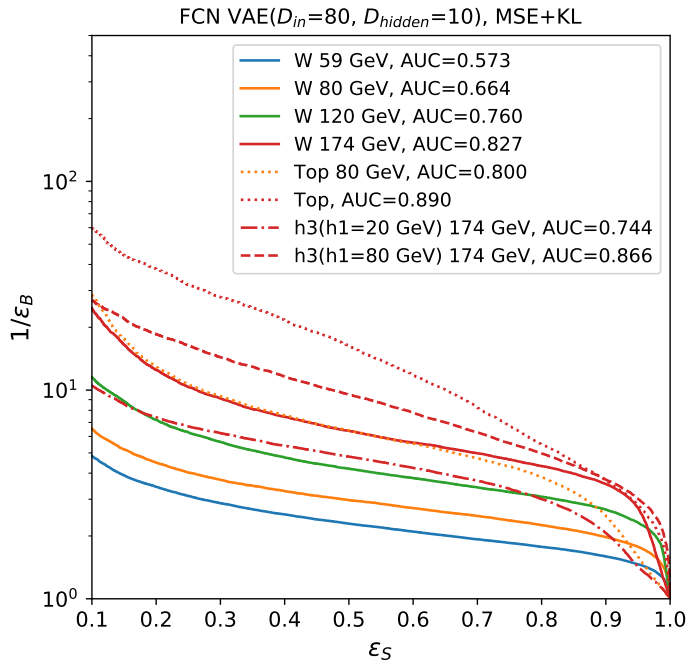


FIG. 8: ROC curves for different jet types, with NLL as the anomaly score. Colors are used to denote jet masses, while different line styles are used for different jet types. We have solid lines for W jets, and red indicates the benchmark mass of 174 GeV for any jet types.

difficulties in tagging jets with lower masses. For instance, W jets with a mass of 80 GeV can only reach the AUC of ~ 0.68 in the best case. We will see how this can be amended in later sections.

IV. MASS DECORRELATION

As mentioned in previous sections, MSE-based autoencoders, be it built with four vectors or in the format of images, are highly correlated with jet mass, when tagging anti-QCD anomalies. In Fig. 10, we show the mass-scuplting effects of reconstruction error based tagger. Higher reconstruction error selects a sample of high-mass QCD jets.

Mass decorrelation is thus an important topic in general searches for resonances with large-radius jets. For example, the bump-hunting analysis utilizes orthogonal information w.r.t. jet mass to reduce the background and then carries out a bump search in the mass dimension. So we dedicated a study to mass-decorrelated taggers in this section. Previous

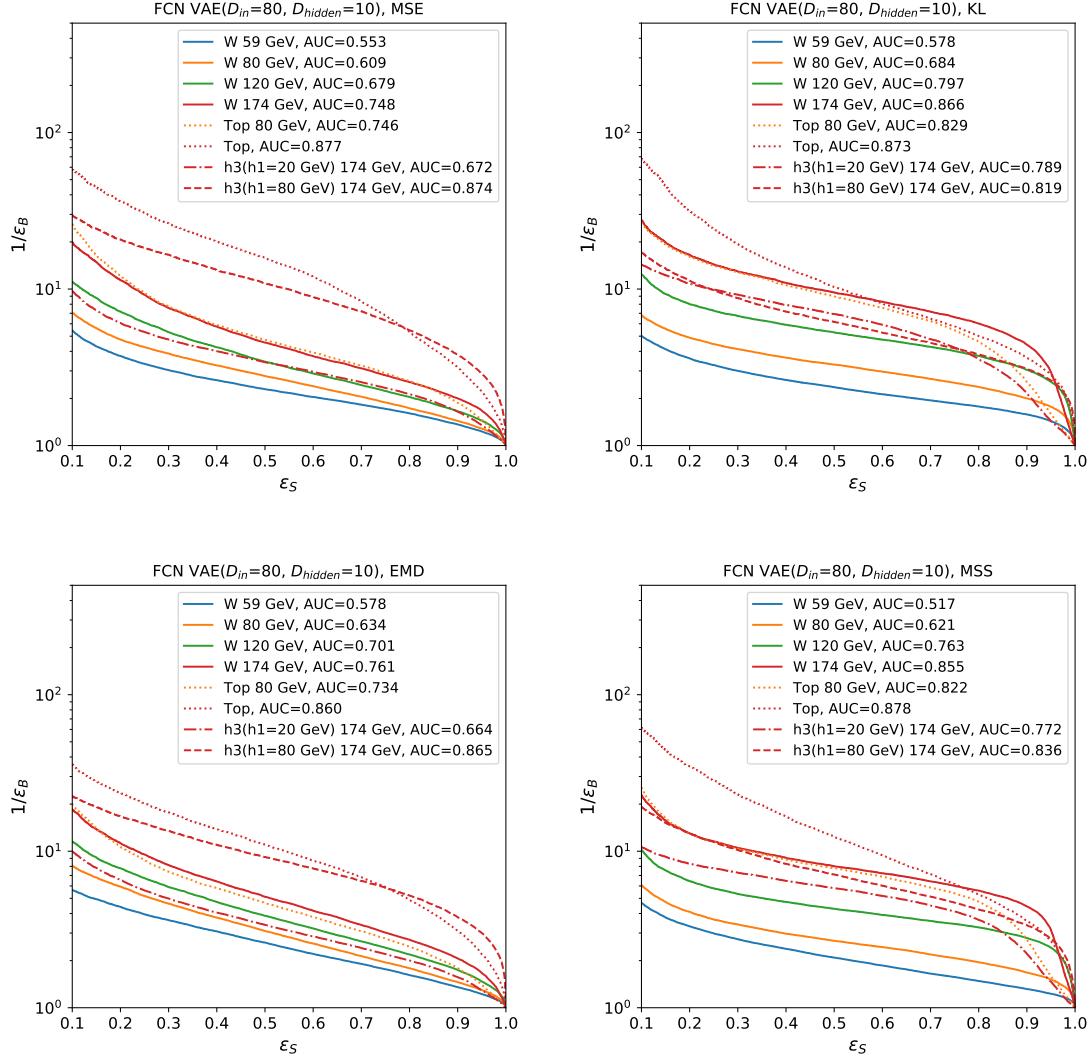


FIG. 9: ROC curves for different jet types, with anomaly metric of MSE reconstruction error (Upper-left), KL divergence (Upper-right), EMD (Lower-left) and MSS (Lower-right), respectively.

works have utilized adversarial training to decorrelate jet mass for either classifiers [15, 16, 26, 27] or autoencoders [6]. However, adversarial training is difficult to tune and takes much more computational resources. We instead employ the distance correlation (DisCo) regularization [14] as a mass-decorrelation baseline.

a. DisCo-VAE In DisCo approach, a distance correlation regularization term is added to the VAE loss as indicated in Eq. 7.

$$\mathcal{L}_{\text{DisCo-VAE}} = \mathcal{L}_{\beta\text{-VAE}} + \kappa R_{\text{DisCo}}, \quad (7)$$

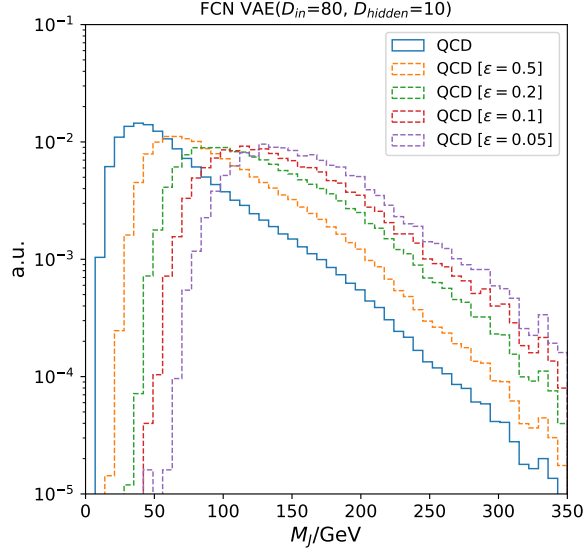


FIG. 10: QCD background mass distribution under different cuts for the background efficiency ϵ on the VAE reconstruction error.

where the regularizer R_{DisCo} is defined in Eq. 8 as the distance correlation between the VAE loss and the jet mass. Distance correlation is a measure of the non-linear correlation between two variables. Independent variables will give a distance correlation of 0.

$$R_{\text{DisCo}} = \text{dCor}(m_J, \mathcal{L}_{\beta\text{-VAE}}) \quad (8)$$

Distance correlation between variable X and Y is defined as in Eq. 9, with the normalized distance covariance in Eq. 10, where (X', Y') and (X'', Y'') are independent and identically distributed samples of (X, Y) .

$$\text{dCor}(X, Y) = \frac{\text{dCov}^2(X, Y)}{\sqrt{\text{dVar}(X)\text{dVar}(Y)}} \quad (9)$$

$$\text{dCov}^2(X, Y) = \langle |X - X'| |Y - Y'| \rangle + \langle |X - X'| \rangle \langle |Y - Y'| \rangle - 2 \langle |X - X'| |Y - Y''| \rangle \quad (10)$$

$$= \text{cov}(\|X - X'\|, \|Y - Y'\|) - 2\text{cov}(\|X - X'\|, \|Y - Y''\|) \quad (11)$$

We tested different κ values ($\kappa = 0.1, 0.5, 1, 10, 100, 200, 500, 1000$)³, and found that $\kappa = 100$ gives a balanced result for our VAE model, in the sense that both mass decorrelation and anomaly detection capability are maintained. We simply employ NLL as the anomaly score here. In Fig. 11, we show mass decorrelation effects for DisCo-VAE with $\kappa = 100$ and $\kappa = 1000$ respectively.

Although $\kappa = 1000$ gives very good mass decorrelation, we find that is not able to preserve good enough anomaly detection capability. In Fig. 12, we present the AUCs after mass-decorrelation for DisCo-VAEs. For all test sets, poor anomaly detection performance is observed compared to the results presented in Fig. 8 and 9. There are even a few test sets giving AUCs less than ~ 0.5 , which again reminds us of the failure case discussed in the last section.

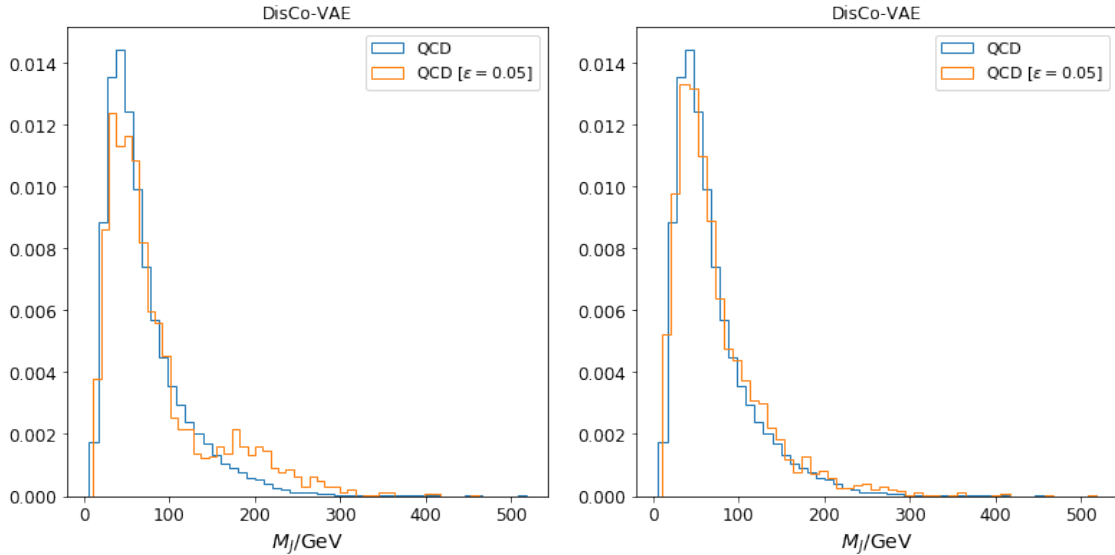


FIG. 11: Mass decorrelation effects for $\kappa = 100$ (Left) and $\kappa = 1000$ (Right).

V. SEMI-SUPERVISION – OE-VAE

As is shown in previous sections, the current situation is that mass-correlation is strong for simple VAEs and mass-decorrelated DisCo-VAE tagger has poor discrimination performance in the full test spectrum. And there are cases that OoD samples are even assigned higher

³ Annealing training is also applied here

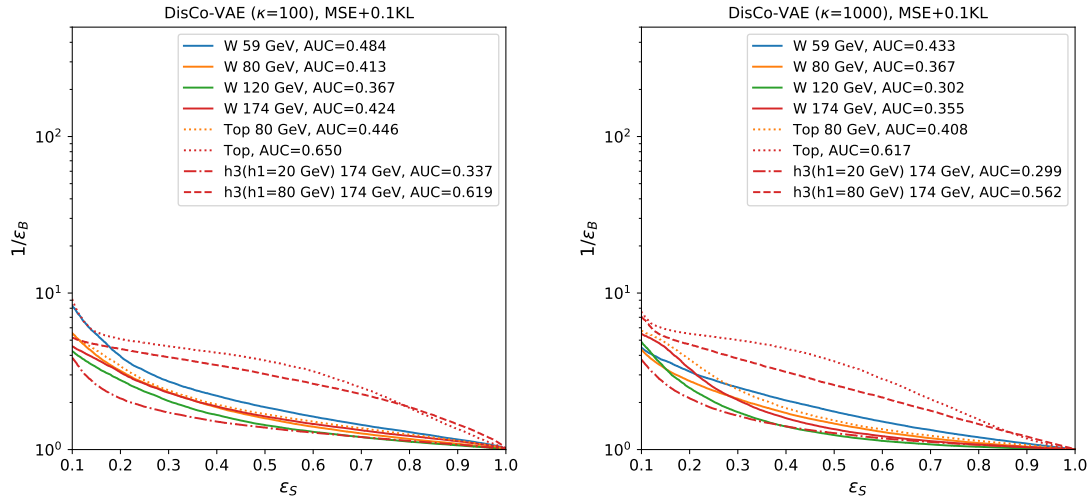


FIG. 12: DisCo-VAE ROC curves for $\kappa = 100$ (Left) and $\kappa = 1000$ (Right).

probability than InD samples. Since unsupervised learning might find bad minima for which not much discriminating power is enabled, semi-supervised learning may help with this problem. One approach which might help with gaining high sensitivity in anomaly detection is Outlier Exposure [13] (OE). OE is similar to training an auxiliary-classifier, in a pseudo-binary manner for which inliers and outliers are required to be separable. Outlier Exposure injects some OoD samples in the training process. This somehow is similar to combining classification with the representation learning process.

We try to achieve two goals at the same time: increasing sensitivity to out-of-distribution samples, and decorrelating the jet mass. By simply exposing outliers to the VAE training, we hope to obtain a general sensitivity increase. Another advantage of having an outlier dataset is that we thus have a handle to provide extra guidelines for our training tasks. A simple and useful practice is that we can match the mass distribution of inlier samples and outlier samples to successfully decorrelate the jet mass. This is a very simple yet powerful trick under the current problem setting.

The outlier samples can be a very good handle to help regularize or shape the minima the VAE finds. We employ mass-rescaled boosted W jet samples as outliers exposed to the VAE training process. As mentioned in Section II, boosted W jets are produced by rescaling Standard Model W jet mass. We resampled the mixed W jets to match the mass distribution to the QCD samples. This procedure is similar to the classical approach “planning” [15]. One

may of course use other modern techniques to decorrelate mass. However, in the setting of outlier exposure, it comes naturally to take advantage of the outlier dataset.

In general, the learning objective for OE can be written as adding a penalty term to the original loss term, in Eq. 12.

$$\mathcal{L} = \mathbb{E}_{(x \sim D_{in})} \mathcal{L}_{\beta\text{-VAE}}(x, \hat{x}) + \lambda \mathbb{E}_{(x \sim D_{in}, x' \sim D_{OE})} \mathcal{L}_{OE}(\hat{x}, \hat{x}'), \quad (12)$$

where λ controls the relative strength of OE. The OE loss \mathcal{L}_{OE} gains its concrete form according to tasks at hand.

For convenience, we rewrite the OE-VAE objective as $\mathcal{L}_{OE\text{-VAE}} = \mathcal{L}_{\beta\text{-VAE}} - \lambda \mathcal{L}_{OE}$. The outlier exposure can be performed either in the input space or in the latent space.

- **MSE-OE:** in input space, the OE loss can be written in the sigmoid activation of the difference between reconstruction error of InD samples and OoD samples. This is very similar to an auxiliary task of classification between InD and OoD:

$$\mathcal{L}_{OE} = \text{sigmoid}(\text{MSE}_{\text{OoD}}(x', \hat{x}') - \text{MSE}_{\text{InD}}(x, \hat{x})) \quad (13)$$

- **KL-OE:** we assume that the geometry would be flattened and more linearized in the latent space. It is thus reasonable to employ the margin loss as follows:

$$\mathcal{L}_{OE} = \min\{0, D_{\text{KL}, \text{OoD}}(z') - D_{\text{KL}, \text{InD}}(z) - \text{margin}\} \quad (14)$$

This will encourage outlier samples to have larger loss above a specific margin.

Of course these are not unique choices for OE losses. But they have been effective in our studies.

a. Training Setup We exposed 120,000 OoD samples consisting of boosted (mass-rescaled) W jets, which are resampled to match the mass distribution of the QCD background. Increasing λ puts higher weight on supervision and at the same time enforces stronger mass-decorrelation. Thus $\lambda = 500$ was chosen for MSE-OE accordingly. For KL-OE, we have $\lambda = 2$ and `margin` set to 1 according to mean values of the KL divergence. We cyclically anneal λ ⁴ in the training process to achieve a better balance between the

⁴ Slowly increase λ from 0 to the target value multiple times.

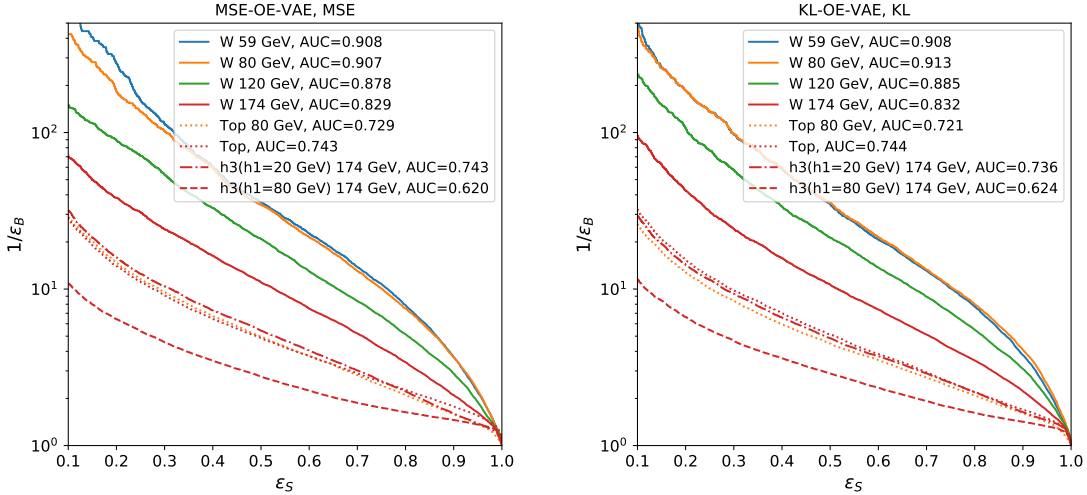


FIG. 13: **Left:** ROC curves for MSE-OE ($\lambda = 500$); **Right:** ROC curves for KL-OE ($\lambda = 2$, $\text{margin} = 1$).

optimization of the VAE loss and the OE loss. The OE training can be applied either from scratch or in the manner of fine-tuning a pre-trained VAE model. We report results for the models that were trained from scratch in the following.

b. Results In Fig. 13, we present ROC curves for different jet types after OE training for MSE-OE and KL-OE respectively. The left panel shows ROC curves for MSE-OE. We accordingly employ simply mean-squared reconstruction error as the anomaly score. The first thing obvious is that W tagging performance is immediately improved. Respectively, a few test sets such as top have lower AUCs compared to Fig. 8 and 9. This is mainly due to the extra mass-decorrelation.⁵ The right panel of Fig. 13 presents ROC curves for KL-OE, for which the KL divergence in latent space is the anomaly score. Generally speaking, the performance is very similar to MSE-OE.

We then examined mass decorrelation effects for OE-VAEs. The results are shown in Fig. 14 for MSE-OE and KL-OE respectively. Excellent mass decorrelation effects are achieved in both scenarios. One thing to keep in mind is that only outlier exposed metrics can be used for mass-decorrelated taggers. For instance, MSE-OE VAE used with KL-based anomaly

⁵ This can be further justified from the comparison with the results of DisCo-VAE, for which only mass-decorrelation effects was introduced. Mass-decorrelation generally drops the AUCs of high mass jets. In comparison, the semi-supervision gains a bit more discrimination for top.

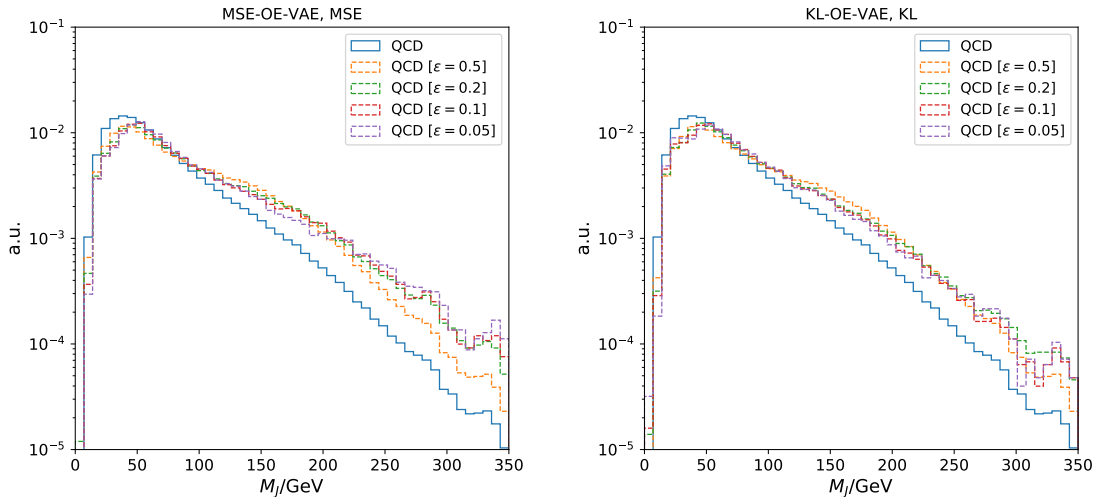


FIG. 14: Mass decorrelation effects in MSE-OE (Left) and KL-OE (Right).

detection will not effectively achieve mass decorrelation. The equivalent “planning” effects only affects one space: input space or latent space. Thus one should match the anomaly metric with the OE scenario, i.e., if one trains OE in the input space, then accordingly using input space MSE anomaly metric will provide the desired mass decorrelation.

c. DisCo-VAE vs OE-VAE To see more clearly how much performance can be achieved by OE-VAE, we compare with DisCo-OE which is also mass-decorrelated. To make a more quantitative examination of mass-decorrelation quality, we employ the measure based on Jensen-Shannon Divergence (JSD, Eq. 15), which is the symmetric version of KL Divergence to measure the similarity between two probability distributions. Generally speaking, the lower JSD is, the better two distributions match. So for an anomalous jet tagger, we expect a low JSD, at the same time a high AUC.

$$D_{\text{JS}}(p(m)||p'(m)) = \frac{1}{2}(D_{\text{KL}}(p(m)||\bar{p}(m)) + D_{\text{KL}}(\bar{p}(m)||p(m))), \quad \bar{p}(m) = \frac{p(m) + p'(m)}{2} \quad (15)$$

In Fig. 15. We plot inverse JSD w.r.t. signal efficiency at background efficiency 5% for the Top test set. OE-VAEs generally will have much higher signal efficiency w.r.t. DisCo-VAEs at the same mass-decorrelation level. It’s promising that OE-VAEs retained very good anomaly detection power while at the same time being mass-decorrelated.

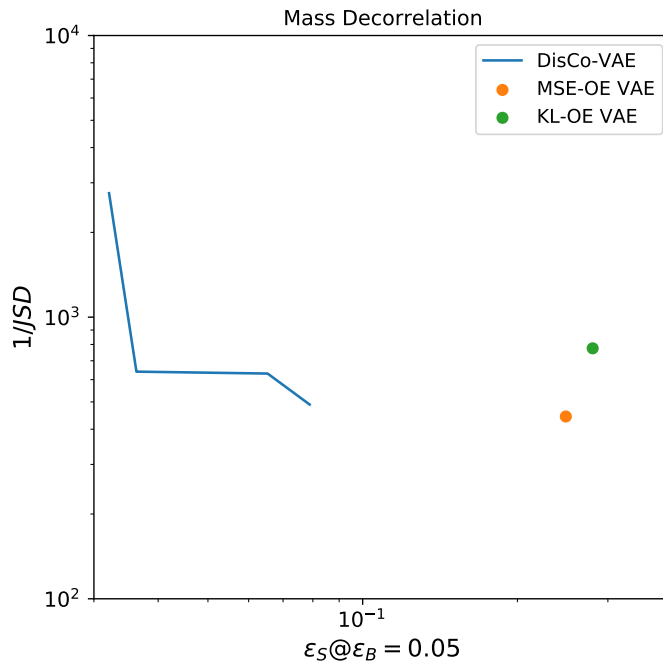


FIG. 15: Jensen-Shannon Divergence vs Signal Efficiency for mass-decorrelated VAEs. Different κ values (100, 200, 500, 1000) are shown for DisCo-VAE.

VI. SUMMARY AND DISCUSSIONS

Unsupervised learning is a potential approach for model-independent new physics searches at the LHC. We carefully investigated Variational Autoencoders for non-QCD anomalous jet tagging. To better regularize the latent space and achieve a good balance between reconstruction error and latent space inference, we cast the work in a generalized VAE setting – β -VAE. We examined the VAE properties, including reconstruction performance, generation ability, and latent representations, of the trained VAEs. High-level features such as jet p_T and jet mass are reconstructed, and the generative model also performs very well.

To systematically assess the anomalous jet tagging performance, we generated a comprehensive series of test sets including mass-rescaled W jets, Top jets, and Higgs jets, as representatives for prongness. Different anomaly metrics were studied. A strong mass correlation is generally observed with all the anomaly scores, leading to much smaller AUCs for low-mass jets.

As an important application of anti-QCD taggers, heavy resonance searches benefit from

a decorrelated tagger which makes background estimation accessible. Aiming at a mass-decorrelated tagger, we employed the distance correlation method, using distance correlation between jet mass and VAE objective as a regularizer. While eliminating mass sculpting effects, the general performance in anti-QCD tagging has been found to be not very satisfying

To achieve good sensitivity to outliers and at the same time decorrelate the jet mass and the anomaly score, we employed the Outlier Exposure technique to help learn more effective latent representations. By injecting some outlier samples in the manner of auxiliary tasks, sensitivity to outliers is generally increased. By matching outlier mass distribution to inlier QCD mass distribution, we achieved very good mass-decorrelation at the same time. OE-VAE is compared with a baseline DisCo-VAE in a two-dimensional measure of the ability of decorrelating jet mass and detecting anomalies. OE-VAEs are generally gaining much better performance. We found that Outlier Exposure is a very simple yet effective trick for improve the performance of deep generative models, VAEs in this work, in the scope of anomalous jet tagging.

In this work, we formulated the problem of using generative models (specifically Variational Autoencoders) to detect out-of-distribution samples in jet physics. We observed that unsupervised learning without any guidelines will not give the optimal solution for specific tasks. A simple semi-supervised approach to enhance the performance was investigated. Despite this effort, there are still several improvements that could be pursued. In this study, only a simple FCN was used. An LSTM model was also investigated, but not much effort was spent on exploring more complex encoding architectures. We expect improved reconstruction ability in that case. In vanilla VAE, latent priors are simply multivariate Gaussians. This can be extended to more complex latent priors. Besides these, alternative reconstruction errors or input space similarity metrics can be explored to better represent the input space. We leave these possibilities for future work.

Acknowledgments

This work is supported by IVADO Fundamental Research Grant and Natural Sciences and Engineering Research Council of Canada (NSERC). The authors would like to acknowledge Amir Farbin, Debottam Bakshi Gupta, Takuya Nobe, and Johnny Raine for early participation in the project. TC would like to thank Faruk Ahmed, Aaron Courville and

Florian Bordes for helpful discussions on anomaly detection in the general machine learning community.

Appendix A: Regularization Strength affects VAEs behaviour

As discussed in Sec. II, regularization strength β will affect jet reconstruction and also the latent distribution. In Fig. 16, reconstructed jet observables are shown for different $\beta = 0.1, 0.5, 1.0$. When β increases, reconstruction performance drops. In Fig. 17, tSNE visualization of latent representations are shown. As β increases, in latent space there are clustering effects emerging.

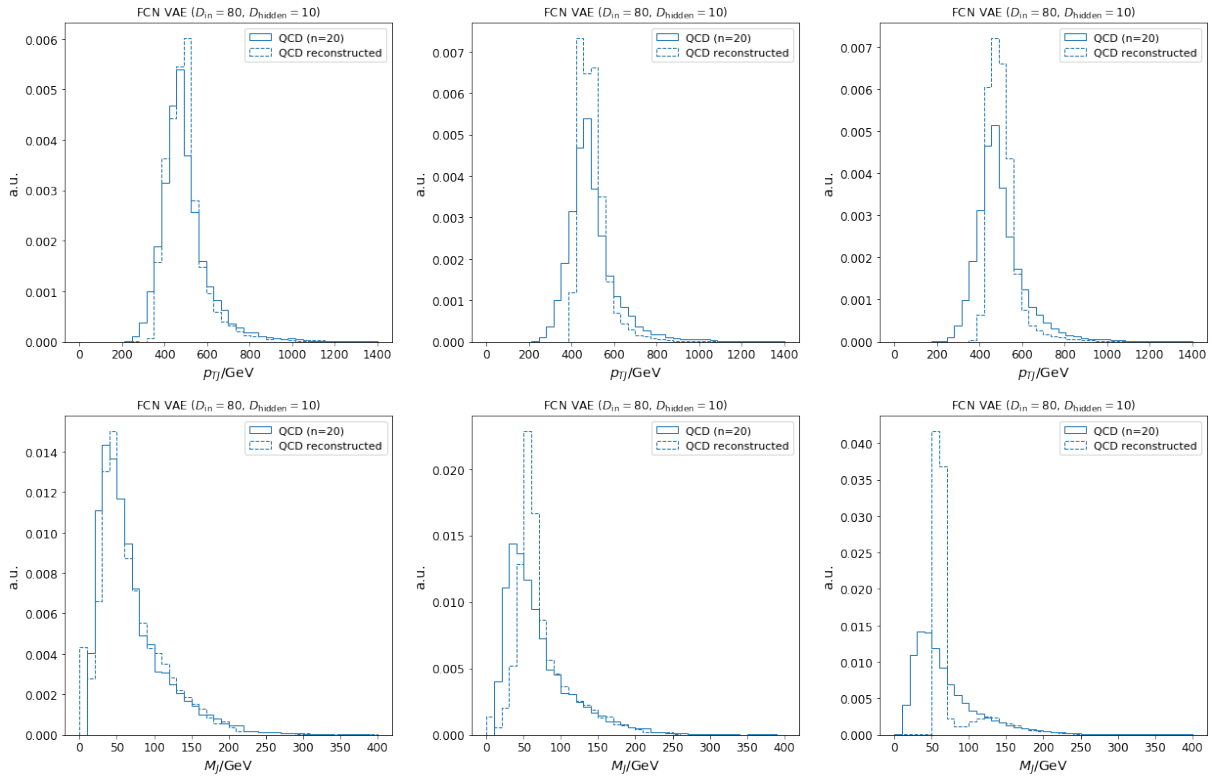


FIG. 16: Reconstructed jet p_T and M_J for different β s. **Left:** $\beta = 0.1$; **Middle:** $\beta = 0.5$; **Right:** $\beta = 1.0$.

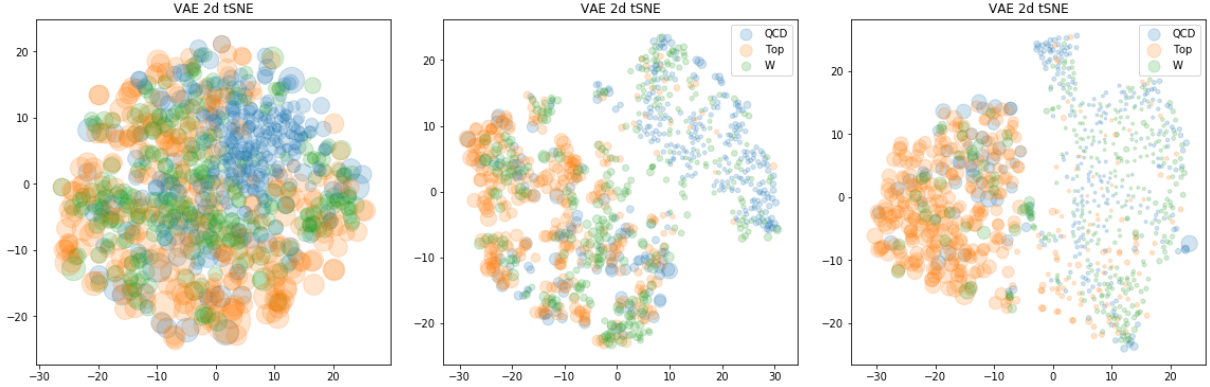


FIG. 17: tSNE visualizations of the latent representations (QCD jets (Blue), W jets (Green) and Top jets (Orange)). **Left:** $\beta = 0.1$; **Middle:** $\beta = 0.5$; **Right:** $\beta = 1.0$.

Appendix B: Supervised W/QCD Classifier vs OE-VAE

Since we utilized an extra W jets dataset in the semi-supervision, it will be interesting to see how the results are compared with supervised W/QCD DNN classifiers. We employ a simple fully-connected DNN architecture ($\text{ReLu}(256) \rightarrow \text{ReLu}(128) \rightarrow \text{ReLu}(64) \rightarrow \text{ReLu}(6) \rightarrow \text{Sigmoid}$), and train with the same datasets and input features as in OE-VAE training⁶. To compare with mass-decorrelated VAE models, we also trained with reweighted samples to decorrelate mass for a supervised W/QCD tagger. Mass decorrelation results are shown in Fig. 18.

ROCs for both taggers are shown in Fig. 19. In general, W/QCD classifier tags W jets with different masses quite efficiently. A mass-decorrelated W/QCD tagger can also be used to tag other jet types, although with sub-optimal performance. This is due to the remaining transferability of supervised taggers [5, 28].

In Fig. 20, we compare tagging performance on held-out classes (Top and Higgs jets) of supervised W/QCD classifier and VAE models. On the left panel, we compare the W/QCD classifier with simple VAE for detecting Top jets and Higgs jets. VAE generally has better performance regarding these held-out classes. However, it's not a completely fair comparison, since both taggers are mass-sculpted. For a fair comparison, we thus compare OE-VAE with

⁶ Class weight is employed to balance dataset size of different classes.

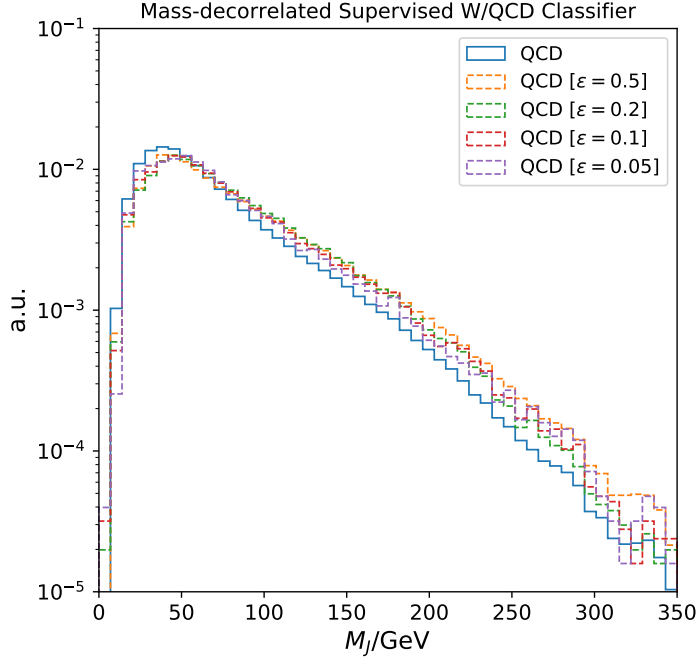


FIG. 18: Mass decorrelation results for mass-decorrelated supervised W/QCD classifier.

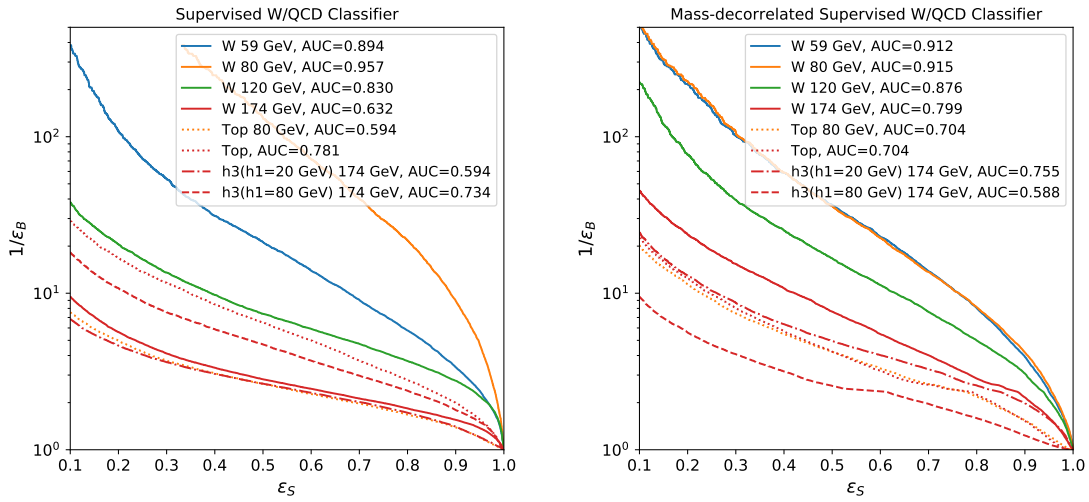


FIG. 19: **Left:** ROCs for supervised W/QCD classifier; **Right:** ROCs for mass-decorrelated supervised W/QCD classifier.

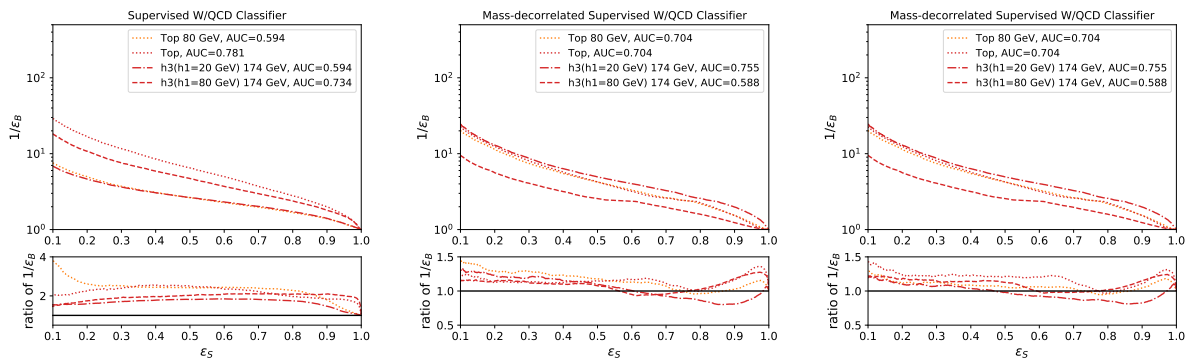


FIG. 20: ROCs for held-out classes. In the upper part, ROCs from (mass-decorrelated) W/QCD classifier are shown, while in the lower part, the ratios of $1/\epsilon_B$ of (OE-)VAEs to W/QCD classifier are presented. **Left:** VAE ; **Middle:** MSE-OE ; **Right:** KL-OE

the mass-decorrelated W/QCD classifier on the middle and right panels of Fig. 20.

-
- [1] Jack H. Collins, Kiel Howe, and Benjamin Nachman. Anomaly Detection for Resonant New Physics with Machine Learning. *Phys. Rev. Lett.*, 121(24):241803, 2018, 1805.02664.
 - [2] Jack H. Collins, Kiel Howe, and Benjamin Nachman. Extending the search for new resonances with machine learning. *Phys. Rev.*, D99(1):014038, 2019, 1902.02634.
 - [3] Jan Hajer, Ying-Ying Li, Tao Liu, and He Wang. Novelty Detection Meets Collider Physics. 2018, 1807.10261.
 - [4] Benjamin Nachman and David Shih. Anomaly Detection with Density Estimation. 2020, 2001.04990.
 - [5] J. A. Aguilar-Saavedra, Jack H. Collins, and Rashmish K. Mishra. A generic anti-QCD jet tagger. *JHEP*, 11:163, 2017, 1709.01087.
 - [6] Theo Heimel, Gregor Kasieczka, Tilman Plehn, and Jennifer M. Thompson. QCD or What? *SciPost Phys.*, 6(3):030, 2019, 1808.08979.
 - [7] Marco Farina, Yuichiro Nakai, and David Shih. Searching for New Physics with Deep Autoencoders. 2018, 1808.08992.
 - [8] Tuhin S. Roy and Aravind H. Vijay. A robust anomaly finder based on autoencoder. 2019, 1903.02032.

- [9] Andrew Blance, Michael Spannowsky, and Philip Waite. Adversarially-trained autoencoders for robust unsupervised new physics searches. *JHEP*, 10:047, 2019, 1905.10384.
- [10] Olmo Cerri, Thong Q. Nguyen, Maurizio Pierini, Maria Spiropulu, and Jean-Roch Vlimant. Variational Autoencoders for New Physics Mining at the Large Hadron Collider. *JHEP*, 05:036, 2019, 1811.10276.
- [11] Diederik P Kingma and Max Welling. Auto-Encoding Variational Bayes. *arXiv e-prints*, page arXiv:1312.6114, Dec 2013, 1312.6114.
- [12] Eric Nalisnick, Akihiro Matsukawa, Yee Whye Teh, Dilan Gorur, and Balaji Lakshminarayanan. Do Deep Generative Models Know What They Don't Know? *arXiv e-prints*, page arXiv:1810.09136, Oct 2018, 1810.09136.
- [13] Dan Hendrycks, Mantas Mazeika, and Thomas Dietterich. Deep Anomaly Detection with Outlier Exposure. *arXiv e-prints*, page arXiv:1812.04606, Dec 2018, 1812.04606.
- [14] Gregor Kasieczka and David Shih. DisCo Fever: Robust Networks Through Distance Correlation. 2020, 2001.05310.
- [15] Performance of mass-decorrelated jet substructure observables for hadronic two-body decay tagging in ATLAS. Technical Report ATL-PHYS-PUB-2018-014, CERN, Geneva, Jul 2018.
- [16] Layne Bradshaw, Rashmish K. Mishra, Andrea Mitridate, and Bryan Ostdiek. Mass Agnostic Jet Taggers. *SciPost Phys.*, 8(1):011, 2020, 1908.08959.
- [17] Johan Alwall, Michel Herquet, Fabio Maltoni, Olivier Mattelaer, and Tim Stelzer. Madgraph 5: going beyond. *Journal of High Energy Physics*, 2011(6), Jun 2011.
- [18] Torbjrn Sjstrand, Stephen Mrenna, and Peter Skands. A brief introduction to pythia 8.1. *Computer Physics Communications*, 178(11):852867, Jun 2008.
- [19] J. de Favereau, C. Delaere, P. Demin, A. Giammanco, V. Lematre, A. Mertens, and M. Selvaggi. Delphes 3: a modular framework for fast simulation of a generic collider experiment. *Journal of High Energy Physics*, 2014(2), Feb 2014.
- [20] Matteo Cacciari, Gavin P Salam, and Gregory Soyez. The anti-kt jet clustering algorithm. *Journal of High Energy Physics*, 2008(04):063063, Apr 2008.
- [21] Irina Higgins, Loïc Matthey, Arka Pal, Christopher Burgess, Xavier Glorot, Matthew M Botvinick, Shakir Mohamed, and Alexander Lerchner. beta-vae: Learning basic visual concepts with a constrained variational framework. In *ICLR*, 2017.
- [22] Diederik P. Kingma and Jimmy Ba. Adam: A method for stochastic optimization, 2014,

1412.6980.

- [23] Laurens van der Maaten and Geoffrey Hinton. Visualizing data using t-SNE. *Journal of Machine Learning Research*, 9:2579–2605, 2008.
- [24] G.C. Branco, P.M. Ferreira, L. Lavoura, M.N. Rebelo, Marc Sher, and Joao P. Silva. Theory and phenomenology of two-Higgs-doublet models. *Phys. Rept.*, 516:1–102, 2012, 1106.0034.
- [25] Patrick T. Komiske, Eric M. Metodiev, and Jesse Thaler. Metric Space of Collider Events. *Phys. Rev. Lett.*, 123(4):041801, 2019, 1902.02346.
- [26] Chase Shimmin, Peter Sadowski, Pierre Baldi, Edison Weik, Daniel Whiteson, Edward Goul, and Andreas Sgaard. Decorrelated Jet Substructure Tagging using Adversarial Neural Networks. *Phys. Rev. D*, 96(7):074034, 2017, 1703.03507.
- [27] Gilles Louppe, Michael Kagan, and Kyle Cranmer. Learning to Pivot with Adversarial Networks. 11 2016, 1611.01046.
- [28] Taoli Cheng. Interpretability Study on Deep Learning for Jet Physics at the Large Hadron Collider. In *33rd Annual Conference on Neural Information Processing Systems*, 11 2019, 1911.01872.